

Article

An Improved Artificial Potential Field Method for Ship Path Planning Based on Artificial Potential Field—Mined Customary Navigation Routes

Yongfeng Suo ¹, Xinyu Chen ^{1,*} , Jie Yue ¹, Shenhua Yang ¹ and Christophe Claramunt ² 

¹ Navigation College, Jimei University, Xiamen 361021, China; suoyongfeng@gmail.com (Y.S.); jjieyue@outlook.com (J.Y.); yangshh@jmu.edu.cn (S.Y.)

² Naval Academy Research Institute, 29240 Brest, France; christophe.claramunt@gmail.com

* Correspondence: 202111823007@jmu.edu.cn

Abstract: In recent years, the artificial potential field has garnered significant attention in ship route planning and traffic flow simulation. However, the traditional artificial potential field method faces challenges in accurately simulating a ship's customary route and navigating experience, leading to significant deviations in prediction results. To address these issues, in this study, we propose an innovative method for simulating and predicting ship traffic flow, building upon the artificial potential field approach. We introduce an AIS track heat map based on the kernel density function and enhance the artificial potential field model by incorporating factors, such as ship navigation habits and ship size. Through a comparison of traffic flow changes before and after the construction of a wind farm, the optimized model demonstrates its effectiveness in improving the accuracy of prediction results.

Keywords: artificial potential field; trace heat map; customary route; route planning; kernel density



Citation: Suo, Y.; Chen, X.; Yue, J.; Yang, S.; Claramunt, C. An Improved Artificial Potential Field Method for Ship Path Planning Based on Artificial Potential Field—Mined Customary Navigation Routes. *J. Mar. Sci. Eng.* **2024**, *12*, 731. <https://doi.org/10.3390/jmse12050731>

Academic Editor: Xinqiang Chen

Received: 12 March 2024

Revised: 26 April 2024

Accepted: 26 April 2024

Published: 27 April 2024



Copyright: © 2024 by the authors. Licensee MDPI, Basel, Switzerland. This article is an open access article distributed under the terms and conditions of the Creative Commons Attribution (CC BY) license (<https://creativecommons.org/licenses/by/4.0/>).

1. Introduction

As a common method for local path planning, the artificial potential field offers advantages in providing fast, convenient, and practical navigation solutions. However, most existing artificial potential field path planning models are tailored to urban network contexts and do not directly translate to maritime settings. Few studies have comprehensively addressed the impact of the navigation experience and customary routes on ship navigation. With the emergence of extensive maritime data, it has become possible to infer customary navigation behaviors and integrate subjective factors such as navigation experience into route planning processes. This presents valuable datasets for reference, where navigation experiences can be inferred to a certain extent. Subsequently, it opens up opportunities to search for optimal trajectories based on past behaviors and current navigation contexts.

The objective of the research presented in this paper is to enhance an artificial potential energy algorithm by introducing a customized route gravitational field that considers the impact of historical experience on route planning. The contributions of this research are twofold. Firstly, we refine the artificial potential field model, incorporating the effects of navigation experience grounded in traditional methods. This model simulates and predicts navigation routes based on both conventional and current conditions, encompassing obstacle avoidance. Secondly, the entire modeling framework undergoes testing in the surrounding area of the Pinghaiwan Offshore Wind Farm, and its feasibility is assessed through the practical implementation of the optimized model. The artificial potential field model seamlessly integrates with actual geographic and maritime data. Moreover, the refined sea navigation simulation model of the artificial potential field is fully aligned with the spatiotemporal characteristics of the AIS system to mimic traffic flow.

1.1. Related Work

In recent years, there have been many in-depth studies in the field of traffic flow simulation and trajectory prediction. In order to solve the challenges inherent in the complexity and dynamic growth of VTF time series, a new hierarchical method for VTF prediction is proposed [1]. Considering the heterogeneity of traffic flows, a new “Space and Channel Recalibration” (SCR) module was designed to analyze the correlation contribution accurately [2]. A spatiotemporal traffic flow prediction model based on the combination of a graph attention network (GAT) and bidirectional gated cycle unit (BiGRU) neural network was proposed [3]. A dynamic remapping neural network (DMGNN) integrated with traffic accidents is proposed for multi-step traffic flow prediction [4]. A Generic Dynamic Graph Convolutional Network (GDGCN) for traffic flow prediction is proposed [5]. A nuclear extreme learning machine (GA-KELM) improved by a genetic search algorithm is proposed to exploit its potential to improve the prediction accuracy and generalization performance [6]. Pso-bi is based on the combination of Particle Swarm Optimization (PSO) and Bidirectional Long Short-Term Memory (Bi-LSTM) neural networks; this is the LSTM short-term traffic flow prediction model [7]. The short-term traffic flow prediction model is constructed by using a short-term memory network, and the mode aliasing problem is solved by variational mode decomposition [8]. A new deep learning model, a graph space–time channel unit (U-shaped network) is proposed to achieve accurate and reliable traffic flow predictions [9]. This problem is dealt with by combining the idea of neural ODEs and modeling the change rate of traffic flow on urban roads [10].

The general local path planning method should not be applied to the complex marine navigation environment; some algorithms consider the speed and course of other ships unchanged [11,12], but this is not completely appropriate in many situations. A valuable alternative is provided by the artificial potential field, which has a simple structure; it is also easy to understand and implement. This method abstracts and models environmental information into a series of reference locations, and it is suitable for ship dynamic path planning. The artificial potential field has been widely used in path planning and motion simulation [13].

Over the past few years, several methods have been proposed to solve the problem of unattainable goals [14]. The target unreachable problem can be solved by adjusting the repulsion angle and safety distance factor [15]. An improved algorithm and objective function solve the problem of the local optimal solution [16]. A new predictive artificial potential field has been developed, using time information and predicted potential to plan smoother paths and verify the accessibility of local minimum and other enhanced special scenarios through simulation [17]. The improved artificial potential field method takes the target along the exclusive equipotential surface along a shorter feasible path for local optimization [18]. The local minimum point problem is overcome by introducing the second virtual target attraction potential field [19].

Other studies also integrate other algorithms to make up for defects and expand the advantages [20]. An improved artificial potential field method is combined with a cosine adaptive genetic algorithm to realize trajectory optimization under an obstacle environment and improve the efficiency [21]. A new AAPF method based on the APF method and ECPS method solves the multi-objective obstacle avoidance problem by considering the influence of uncertain factors [22]. The potential field method of complex motion alleviates the problems of the obstacle avoidance environment when the degree of freedom increases through the improved numerical algorithm of the Jacobian matrix [23]. The optimal collision-free path planning of multi-object formation combines A* and multi-objective-improved artificial potential field algorithms [24].

In general, compared with other algorithms, the artificial potential energy method has a simple model structure, high precision, and a good simulation effect. It is, therefore, suitable for sea traffic simulation.

1.2. General Remarks

The above literature provides theoretical support for marine traffic-related construction and track planning. The artificial potential field method is generally optimized among the aforementioned works. The local optimal offset problem is also improved. However, there are still some problems that affect its accuracy and reliability in the application of track planning. The existing artificial potential field method can be used for ship autonomous navigation and traffic flow simulation, but it is difficult to simulate ship customary routes and customary navigation methods using this method. This study optimizes an artificial potential field model based on an AIS trajectory thermal map to improve the accuracy of traffic flow prediction. A kernel density function is innovatively introduced to optimize the model, and a thermal map complements the approach by supporting visual representations that facilitate the patterns that appear.

2. Traditional Artificial Potential Field Method

The traditional artificial potential field method originates from the physics concept of potential energy. Its fundamental principle views the objects in space as pixels and perceives the research space as a potential field environment. The target point exerts a strong attractive force, compelling the research object to progressively move toward it. Conversely, obstacles emit repulsive forces. The combination of attractive and repulsive forces creates a potential energy gradient, causing the object to avoid regions of high potential energy. By monitoring variations in the potential energy gradient, we can devise an optimal obstacle avoidance path. A concise analysis of this principle is depicted in Figure 1.

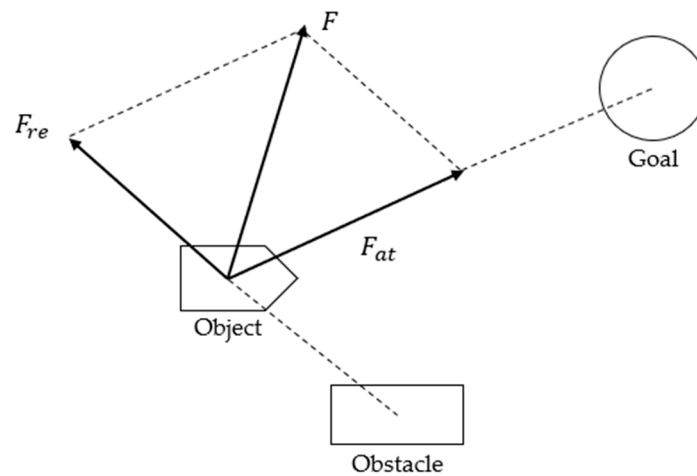


Figure 1. The force analysis of the traditional artificial potential field method.

In Figure 1, F_{at} is the global gravity generated by the goal, F_{re} is the repulsion generated by the obstacle, and F is the resultant force of both. The object will move under the action of this resultant force.

2.1. The Global Gravity

Let OS (own ship) denote a ship, which is located in a grid environment (x, y) ; the global attraction can be obtained from Equation (1):

$$F_{at} = -\alpha[(x - x_1)^2 + (y - y_1)^2] \tag{1}$$

where α is the gravitational coefficient; (x, y) is the coordinate of OS; (x_1, y_1) is the coordinate of the target point and the symbol represents the direction of the force (the attractive force). According to the formula, F_a is inversely proportional to OS and the distance to the target point.

2.2. Obstacle Repulsive Field

When OS is in raster space (x, y) , the repulsive field function is shown in Equation (2):

$$F_{re} = \begin{cases} N \times \left(\frac{1}{d_{re2}} - \frac{1}{D_{re0}} \right) \frac{1}{d_{re2}^2}, & d_{re2} \leq D_{re0} \\ 0, & d_{re2} > D_{re0} \end{cases} \quad (2)$$

where N is the repulsive force directly proportional gain factor. d_{re2} represents the distance from OS to the barrier boundary. D_{re0} is a constant, representing the influence distance of the repulsive field.

2.3. Comprehensive Force Field

The resultant force of the research object should be a vector synthesis of the global gravitational force and the obstacle repulsion function. Therefore, the resultant force equation (Equation (3)) is shown as follows:

$$F = F_{at} + F_{re} \quad (3)$$

3. Improved Artificial Potential Field Method

Based on geographic information and historical AIS data, this study takes the customary route as one of the factors to consider in path planning and improves the artificial potential field model.

Considering that the gravitational force generated by different densities of customary paths should be different, the nuclear density factor is introduced to provide a customary path gravitational field. The denser the tracks, the greater the amount of gravity generated. Therefore, the thermal map drawing based on AIS historical trajectory, which has the characteristics of both two-dimensional spatial coordinates and density function, is introduced and coincides with the elements needed for the construction of a gravitational field. The purpose of this method is to fully mobilize the dynamic spatiotemporal characteristics of the customary route and show them in the model.

The research program of model building is shown in Figure 2.

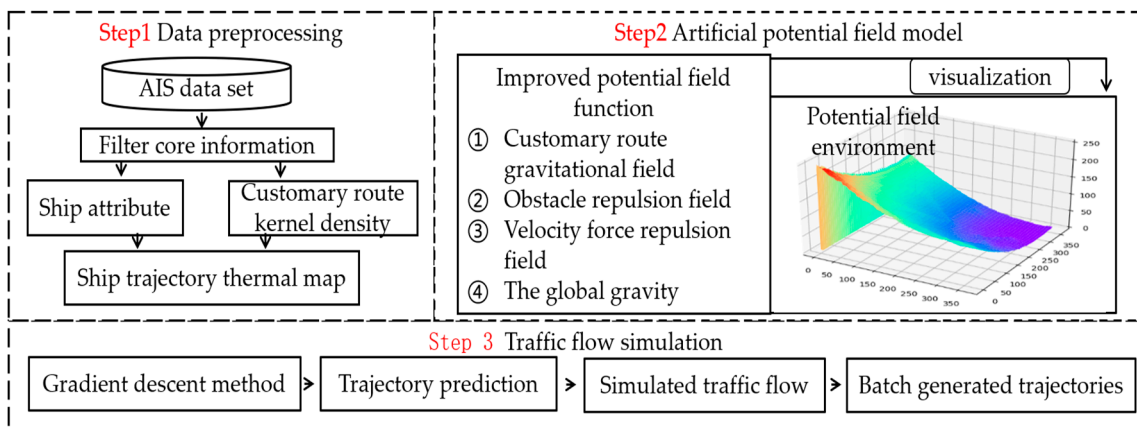


Figure 2. The general process of model establishment.

3.1. Customary Route Gravitational Field

The common artificial potential field model does not consider the effect of the customary route on the ship’s navigation method. To model a customary-route-impacted potential energy field, it is important to search for a route track based on a ship’s history. This can be achieved by fully considering the characteristics of the maritime traffic channel within a certain period, including the ship traffic flow characteristics, traffic flow density, and change trends. By doing so, we can effectively analyze and understand the behavior of ships sailing in the area.

Let OS (own ship) denote a ship, which is located in a grid environment (x, y) , and the customary route gravity function is shown in Equation (4):

$$F_{ar} = \begin{cases} -\sigma \left(\frac{1}{d_{a2}} - \frac{1}{D_{a0}} \right) WP_{hot}, & d_{a2} \leq D_{a0} \\ 0, & d_{a2} > D_{a0} \end{cases} \quad (4)$$

F_{ar} represents the gravitational force generated by stress on a customary route. The symbol σ is the customary airway gravity proportional gain factor, and its value is 14.4. This is to correct the gravity of the customary route to ensure that the target receives enough gravity within the range of the gravitational field while not affecting the leading role of the global gravity and the main purpose of obstacle avoidance. Based on this calculation, its value is obtained. d_{a2} represents the distance between the OS and the customary route path. D_{a0} is a constant, representing the influence of distance of habit. Examples of the above concrete concepts are shown in Figure 3. When the subsequent path deviates far from the original path, it means that the track has been substantially adjusted, the reference value of the historical path is limited at this time, and the model no longer considers its role. The establishment of the model is mainly influenced by global gravity. When there is no significant change in the ship's path on the customary route, the ships tend to travel on the historically optimal path. When the planned route of a ship does not coincide much with the customary route, the customary route has little influence on it.

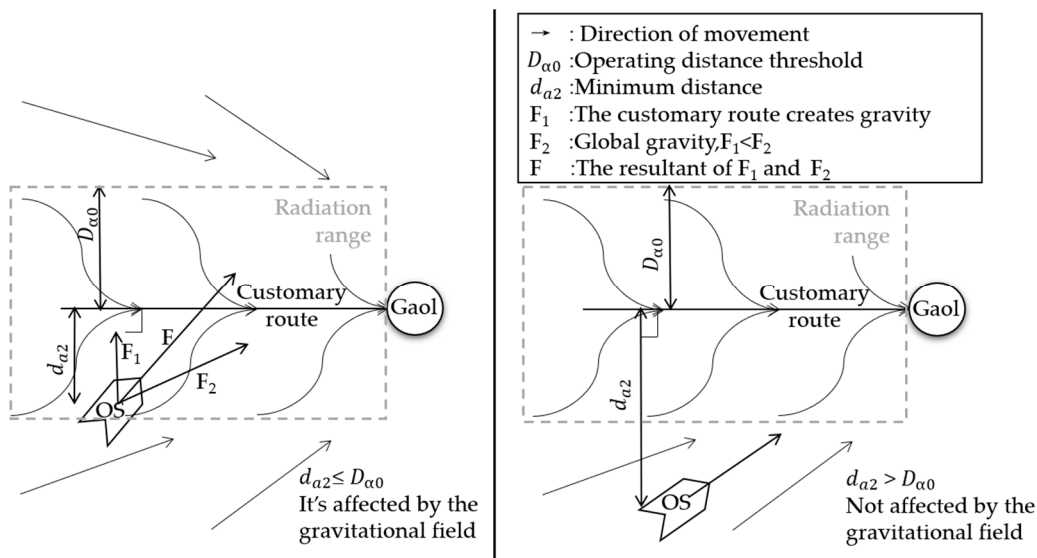


Figure 3. Customary route gravitational field parameters.

AIS data are classified according to different ship types. The influence of different ship types on a route varies. Generally, larger ships tend to follow a certain track-driving habit. Therefore, in this study, ships are divided into five classes based on their gross tonnage. The model introduces a correlation coefficient of uppercase W , which is assigned different values depending on the ship class. The assignment of W values is determined through experimental debugging, and the feasibility of the model will be verified later. Table 1 shows the values assigned to each ship class. Among them, the ship class is divided according to the gross tonnage: first-class ships weigh more than 1600 gross tons, second-class ships 600–1600 gross tons, third-class ships 200–600 gross tons, fourth-class ships 50–200 gross tons, and fifth-class ships less than 50 gross tons. For the above classification, refer to IMO MT-69 (measuring convention).

Table 1. Ship tonnage correlation coefficient W .

Class of Ship	W
First-class ship	0.8
Second-class ship	0.9
Third-class ship	1.0
Fourth-class ship	1.1
Fifth-class ship	1.2

The density distribution of the customary route can be intuitively obtained through the path heat map. The denser the path, the higher the thermal value. Through the three-dimensional thermal map, we can intuitively see a curved surface formed by the density function of the locus kernel. The three-dimensional heat map plane can be obtained by intercepting part of the ballistic heat map, as shown in Figure 4.

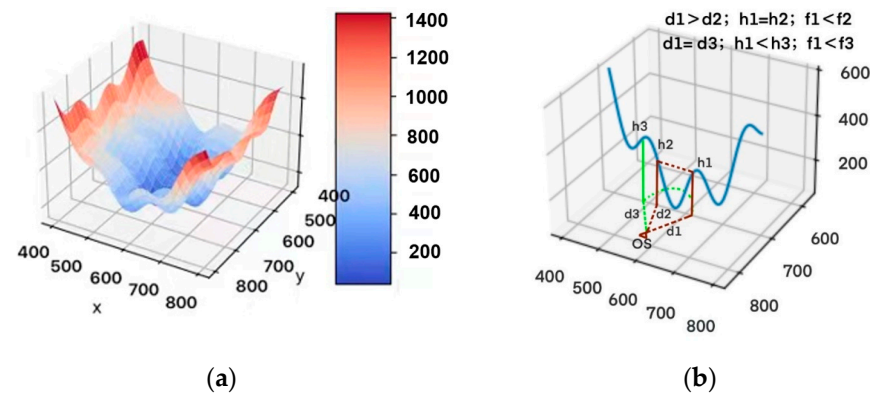


Figure 4. Three-dimensional (3D) thermal diagram: (a) 3D thermal map of customary route; (b) cross-section drawn.

A three-dimensional coordinate system is established on the profile map (b). The x and y axes correspond to the grid environment, and the z -axis represents the height of the thermal value, which can also reflect the density degree of the path. As shown in Figure 4b, the density of the path is positively correlated with the gravity generated at this point, which, together with the relative distance D_{a2} , determines the gravity of the customary route. When the relative distance is certain, the greater the thermal value, and the greater the attraction generated at this coordinate point. Therefore, the thermal coefficient P_{hot} is introduced into the formula, and the value of P_{hot} is based on the thermal value of the corresponding point of the customary route track, as shown in Table 2 (for detailed division). P_{hot} assignment was obtained through experimental debugging, and the feasibility of the model will be verified later.

Table 2. Thermal coefficient P_{hot} .

Thermal Value Partition	P_{hot}
Blue zone (zone 4)	0.8
Green Zone (zone 3)	1.0
Yellow zone (zone 2)	1.2
Red Zone (zone 1)	1.4

3.2. Obstacle Repulsive Field

When OS is in raster space (x, y) , the repulsive field function is shown in Equation (5):

$$F_{re} = \begin{cases} N * \left(\frac{1}{d_{re2}} - \frac{1}{D_{re0}} \right) \frac{1}{d_{re2}^2} (x - x_{r0})^m (x - x_{r0})^n, & d_{re2} \leq D_{re0} \\ 0, & d_{re2} > D_{re0} \end{cases} \quad (5)$$

where N is the repulsive force directly proportional to the gain factor. This is to correct the repulsive force to ensure that the target has enough force when it is close to the obstacle while not affecting the dominant role of global gravity. In addition, it should ensure that, in the case of the gravitational field of the customary route and the repulsive force field of the obstacle being present at the same time, the priority is to ensure that the obstacle is avoided. Based on that, the calculations determined $N = 800$. d_{re2} represents the distance from OS to the barrier boundary. d_{re0} represents the distance from OS to the barrier boundary. D_{re0} is a constant, representing the influence distance of the repulsive field. When the distance between OS and the obstacle is greater than D_{re0} , the repulsive force is zero; that is, the ship is not affected by the repulsive force when it remains at a safe distance from the obstacle. Based on the principle of keeping 5–10 nautical miles between the ship and the coast in the course of sailing, $D_{re0} = 5 \text{ n}$ is any constant greater than zero, and $(x - x_{r0})^m$ is introduced as the distance factor, whose significance is to introduce the relative distance, to ensure that the whole potential field is only globally minimum at the target point. The introduced distance factor of the customary gravitational field, $(x - x_{r0})^n$, indicates that ships preferentially follow the historical customary route in a certain range when avoiding obstacles, where $n \ll m$ ensures that the global gravitational field plays a leading role in the comprehensive force field. The formula $1/D_{re0}$ has the same meaning, which is to limit the repulsive force range of obstacles, and its effect will not be considered in the model once it is out of its radiation range, as shown in Figure 5.

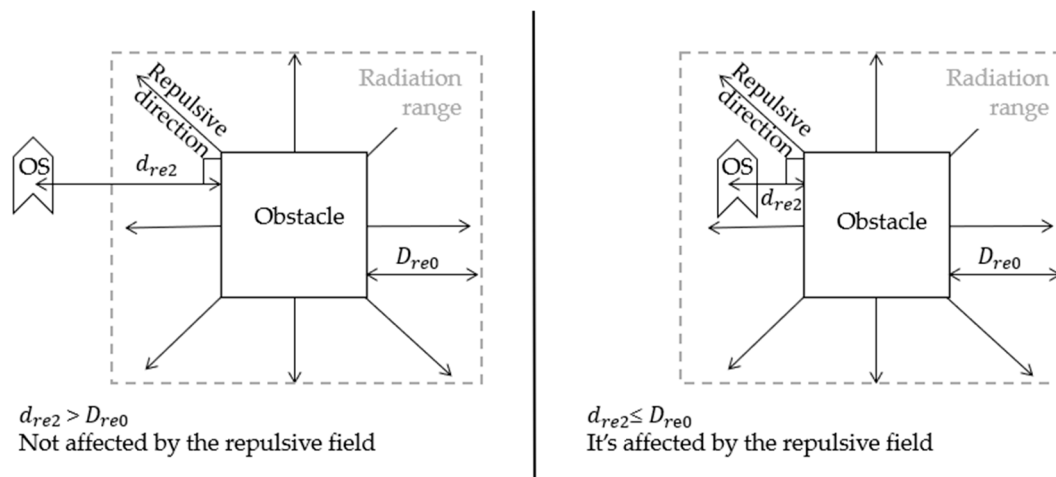


Figure 5. Obstacle repulsive field parameters.

3.3. Velocity Force Repulsion Field

The ship should avoid not only static obstacles but also moving obstacles in the process of sailing. In practical contexts, other ships within a certain range can be identified as dynamic obstacles based on radar and other equipment to obtain real-time data and imaging. We consider the moving ship to be a moving obstacle. When other ships break the preset safety distance, the dynamic obstacle avoidance module in the model is mobilized, and the obstacle boundary coordinates are picked up based on its image. The velocity repulsive force field function is shown in Equation (6):

$$U_{rev} = \begin{cases} \frac{1}{2}R_{rev}, & d_{rev} \leq D_{rev} \cap \alpha \in (-1/2\pi, 1/2\pi) \\ 0, & \text{else} \end{cases} \tag{6}$$

And:

$$R_{rev} = 1/2\varphi_{rev}(v_0 - v_1)^2 \tag{7}$$

In the formula, φ_{rev} is the velocity force proportional gain factor; $v_0 - v_1$ is the relative velocity between the ship and the obstacle. d_{re2} represents the distance from OS to the dynamic obstacle boundary. D_{rev} is a constant, representing the influence distance of the

velocity force repulsion field. When the distance between OS and the obstacle is greater than D_{rev} , the repulsive force is zero; that is, the ship is not affected by the repulsive force when it remains at a safe distance from the obstacle. Based on the principle that ships should maintain a distance of more than two nautical miles from visible obstacles, $D_{rev} = 2$. The direction of the relative velocity is opposite to that of the velocity force exclusion field. α is the angle between the direction of the relative velocity and the vector composed of the ship and the position of the obstacle. Only when $\alpha \in (-1/2\pi, 1/2\pi)$, OS is subjected to the velocity repulsion field. By taking the derivative of the velocity repulsive force field, the route boundary repulsive force function can be obtained. Equation (8) is as follows:

$$F_{rev} = \begin{cases} \varphi_{rev} v e_0, & d_{rev} \leq D_{rev} \cap \alpha \in (-\frac{1}{2\pi}, \frac{1}{2\pi}) \\ 0, & \text{else} \end{cases} \tag{8}$$

Join coefficient e_0 for obstacles needed for the correlation coefficient. The maximum angle range meaning lies in the direction and speed of the ship and the position of the obstacles of the angle between the vector within the scope of radiation. The influence on the speed force field still exists, and we consider the common obstacle avoidance and dynamic obstacle avoidance modules, so the improved artificial potential field model can be set up.

3.4. The Global Gravity

When the target point and starting point are input in the raster space, the objective function potential field function (gravitational potential field function) is shown in Equation (9):

$$U_{at} = 1/2\alpha[(x - x_1)^2 + (y - y_1)^2] \tag{9}$$

The global attraction is the negative gradient of the objective function, which can be obtained from Equation (10):

$$F_{at} = -grad(U_{at}) = -\alpha[(x - x_1)^2 + (y - y_1)^2] \tag{10}$$

where α is the gravitational coefficient, $\alpha = 1/700$; (x, y) is the coordinate of OS, (x_1, y_1) is the coordinate of the target point, and the symbol represents the direction of the force (the attractive force). According to the formula, F_{at} is inversely proportional to OS and the distance to the target point.

3.5. Comprehensive Force Field

Based on previous research, the compound field in the whole raster space can be obtained, which is the sum of the repulsive force field, customary route gravitational field, and global gravitational field. Therefore, the resultant force equation (Equation (11)) is shown as follows:

$$F = F_{ar} + F_{re} + F_{rev} + F_{at} \tag{11}$$

4. Simulation and Results

In this study, we select a certain sea area as the research object and carry out a case analysis.

The case study considered the Pinghaiwan Offshore Wind Farm (under construction) in Putian City as a proof of concept. The planning site of Pinghaiwan Offshore Wind Farm is divided into six areas, from A to F, and the site selection related to this study is denoted by zones C and E. Zone C is a phase II and III project, which will be completed and put into use in 2025, while zone E is a phase IV project, which is still under construction. The specific regional planning of offshore wind farms is shown in Figure 6.



Figure 6. Pinghaiwan Offshore Wind Farm.

Historical AIS data from July 2020 in the study area were selected (before the construction of wind farms in the C and E areas). We constructed the traffic flow simulation model and verified its feasibility. A thermal map of the ship’s path is shown in Figure 7.

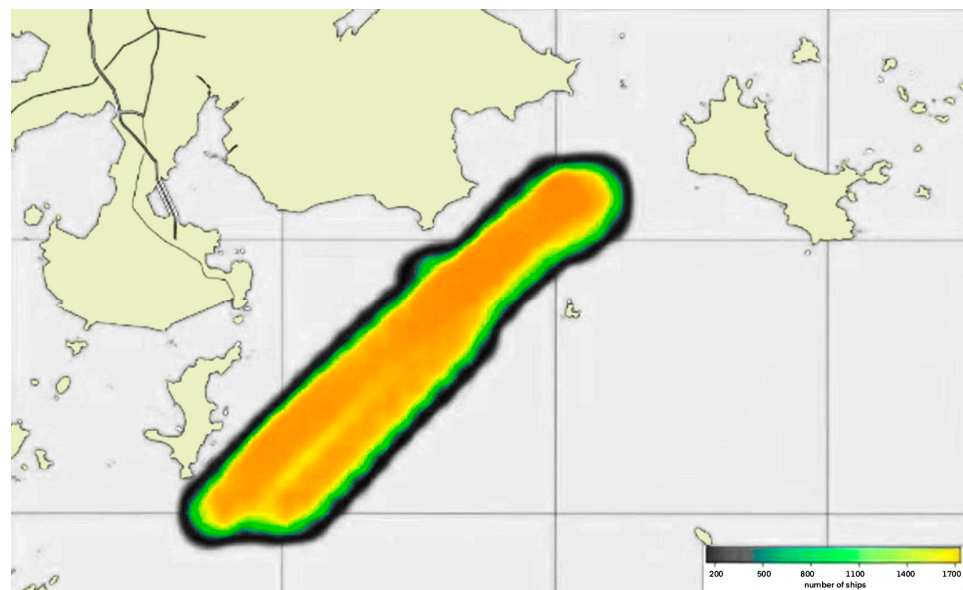


Figure 7. Actual traffic flow around the offshore wind farm (pre-construction).

4.1. Potential Energy Field Establishment

According to the historical AIS data, the customary route gravitational field is established in the raster space region, as shown in Figure 8. It can be seen in Figure 8 that the special point of the historical track generates attraction within a certain radiation range of the surrounding region.

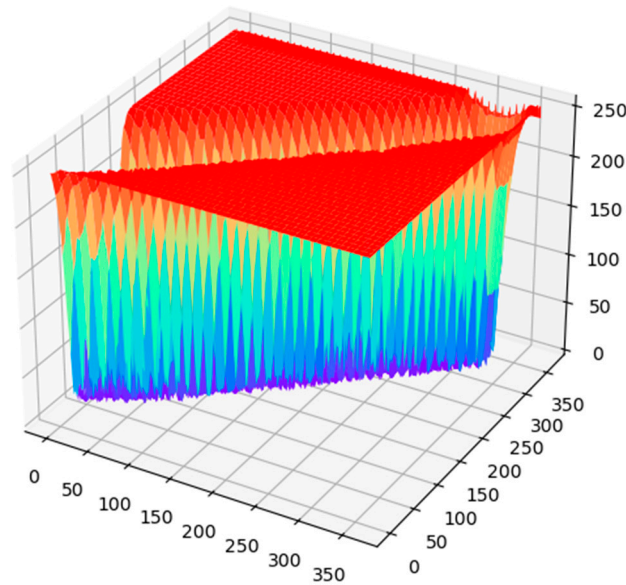


Figure 8. The gravitational field of the customary route.

Based on this customary route gravitational field, the partial derivative of its gravitational function is obtained, and the gradients of the customary route gravitational field in the x and y directions are obtained, respectively. After visualization, a gradient map of the customary route gravitational field is obtained, as shown in Figure 9. The bulge corresponds to the high potential energy, and the depression corresponds to the low potential energy. Thus, a space environment with fluctuations is constructed. There will be some paths that makes the OS transition from high potential energy to low potential energy.

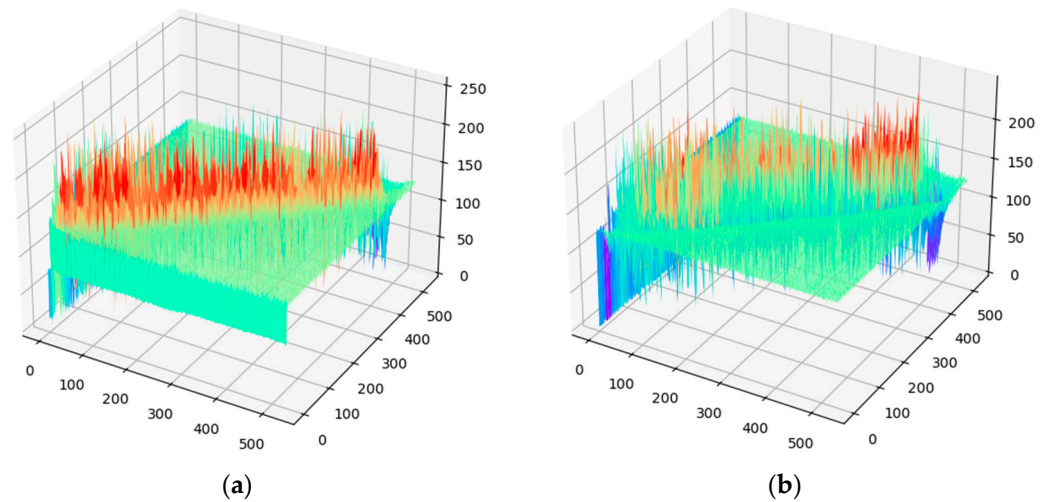


Figure 9. Visualization gradient of the gravitational field in habitual route: (a) gradient (x); (b) gradient (y).

Taking the geographical information of the selected research area, the potential field environment is set, and the barrier of the constructed wind farm is introduced to obtain the repulsive force field, as shown in Figure 10. The special point position of the obstacle in the figure will generate a repulsive force in the surrounding space within a certain radiation range. Based on the above, the global gravity environment is established, as shown in Figure 11. The height difference shown by the three-dimensional surface of the concrete force field is the driving force for the target to advance from the starting point to the endpoint. According to the resultant function shown, the resultant field constructed is shown in Figure 12. The gradient of the force field in the x and y directions was calculated

and visualized, and the visualized gradient function was obtained, as shown in Figure 13. It is the visualization result of the complete potential field environment, showing a surface with ups and downs; the high potential energy is convex, and the low potential energy is concave. The overall trend is that the starting point is inclined to the target point, and there are local fluctuations caused by the repulsion field of obstacles and the gravitational field of the customary route. In this environment, the ship resembles a small ball placed on this surface and always tends to move from high potential energy to low potential energy.

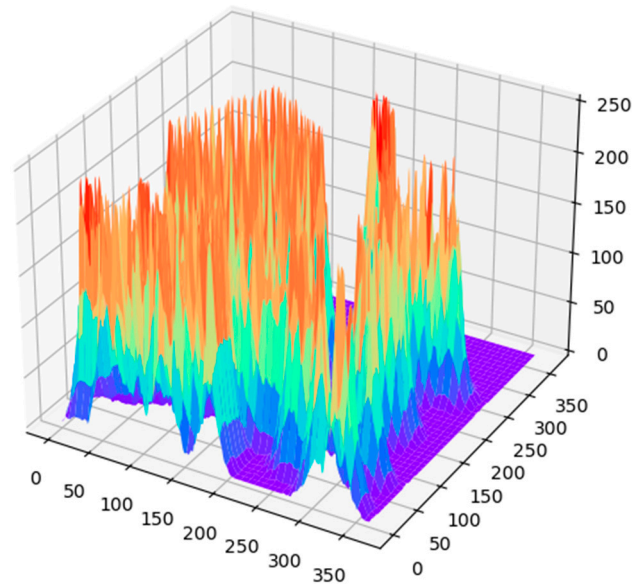


Figure 10. Obstacle repulsive force field.

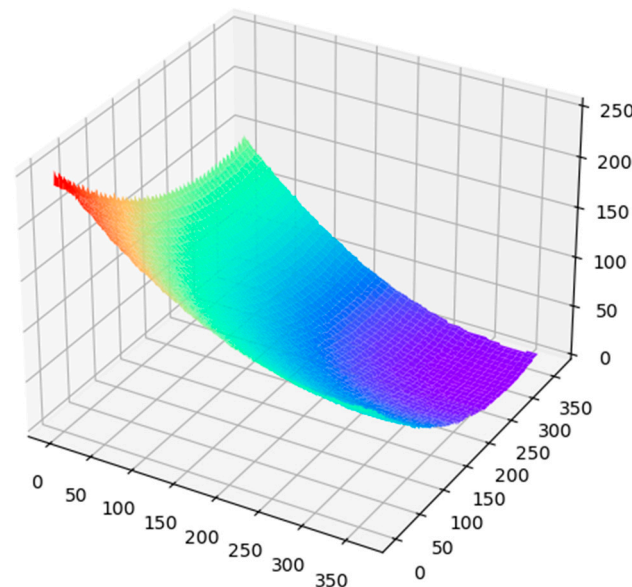


Figure 11. Global gravitational field.

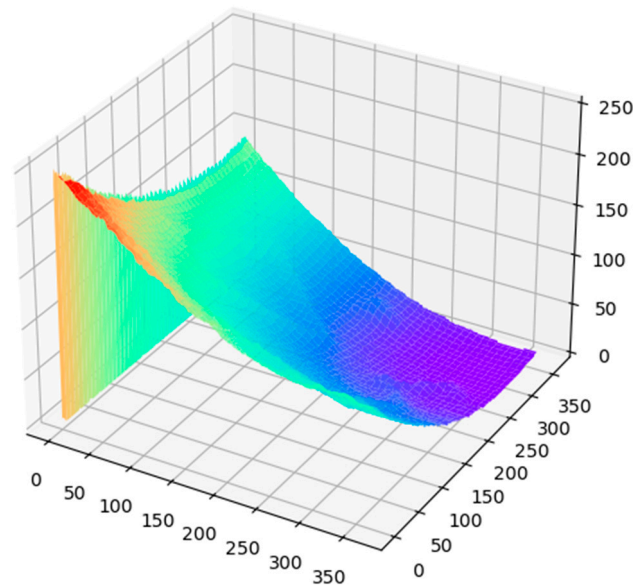


Figure 12. Force field.

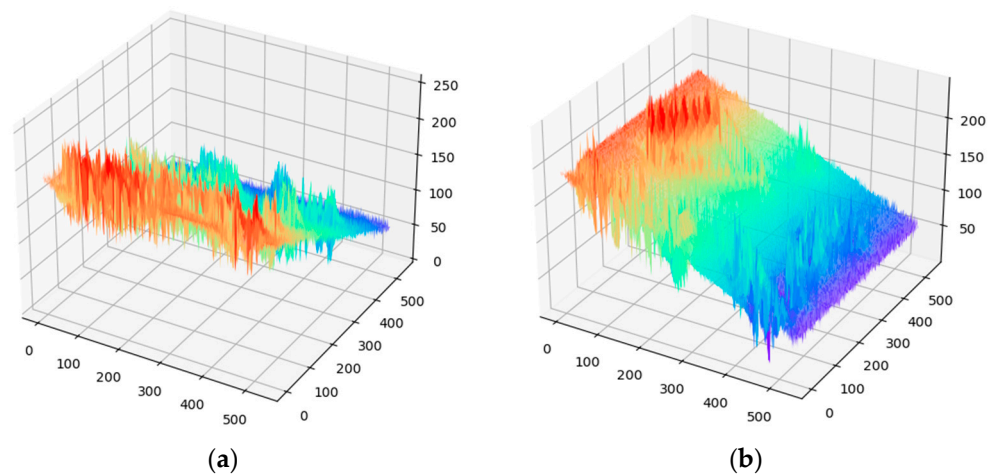


Figure 13. Potential field visualization gradient: (a) potential field visualization gradient (x); (b) potential field visualization gradient (y).

4.2. Traffic Flow Simulation

Under the superposition of each potential energy field, the ship always tends to move from high potential energy to low potential energy to achieve the avoidance goal and obtain the desired planning path. The model is applied to the selected research area, and OS path planning is carried out. A vector diagram of path planning is shown in Figure 14a. The arrow in the figure points from high potential energy to low potential energy, which represents the motion trend of OS. The blue trajectory is the simulated route of the improved model, and the red trajectory is the simulated route of the traditional artificial potential field model. It can be seen that the trajectory of the model before improvement features a large turn, and there is the problem of the target being unreachable. The refined model eliminates the issue of unreachable targets, ensuring smooth trajectories that align with common navigation laws, thereby enhancing the accuracy and reliability of maritime traffic flow simulations.

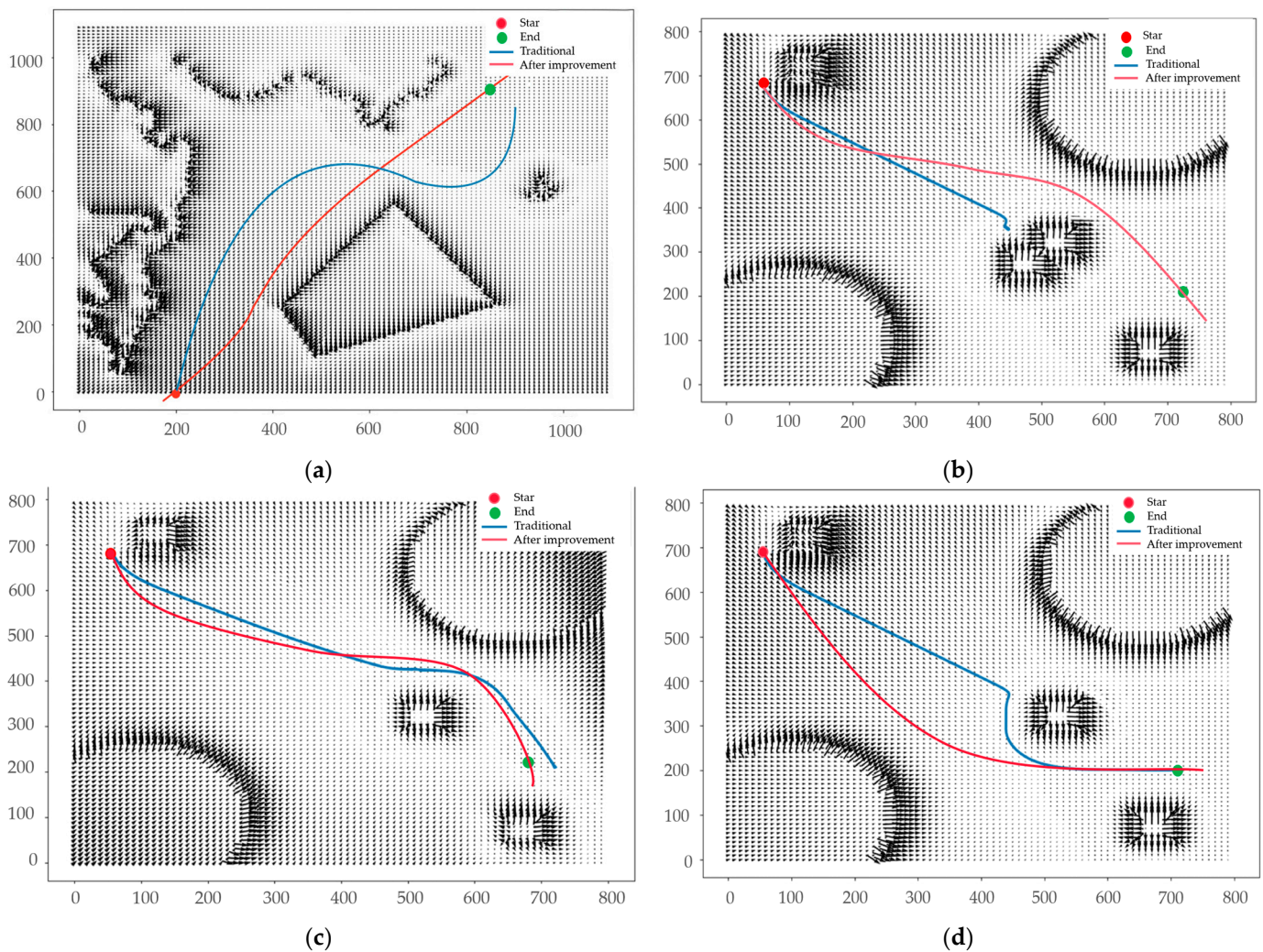


Figure 14. Route planning vector diagram: (a) trajectory simulation 1; (b) trajectory simulation 2; (c) trajectory simulation 3; and (d) trajectory simulation 4.

In order to ensure the feasibility and applicability of the model proposed in this study, the distribution of the model was applied to three different types of obstacles for testing to simulate obstacle avoidance scenarios under different circumstances and to compare with the traditional APF path planning method to verify the feasibility and superiority of the model. The simulation experiment includes the following three scenarios:

(1) Complex U-shaped disorder.

The simulation scenario mainly aims at the problem that the traditional artificial potential field method easily falls into a situation where it cannot escape when it encounters U-shaped obstacles. The simulation results are shown in Figure 14b. In the figure, the blue trajectory represents the traditional artificial potential field model path planning, and the red trajectory represents the improved artificial potential field model path planning. The results show that the simulation effect of the traditional model is not good, but the red path obtained by the improved model can overcome the local limitations and reach the destination relatively smoothly.

(2) The goal cannot be achieved.

In the traditional artificial potential field method, when the obstacle is close to the target point, sometimes the object of study cannot reach the destination (as shown by the blue trajectory in the figure) because the compound force fields cancel each other. After improved path planning, we can adjust to deal with this situation and finally reach the destination smoothly. The simulation results are shown in Figure 14c. In the figure, the

blue trajectory represents traditional artificial potential field model path planning, and the red trajectory represents improved artificial potential field model path planning.

(3) Smoothness optimization.

Compared with the result of traditional artificial potential energy path planning (blue path), the improved path planning method (red path) can obtain a smoother path, which has certain advantages. The simulation results are shown in Figure 14d.

4.3. Traffic Flow Simulation

OS navigates under the joint action of customary route gravitational field and global gravity, offshore wind farm and dynamic ship comprehensive repulsion, etc. Under the superposition of each potential energy field, the ship always tends to move from high potential energy to low potential energy to achieve the avoidance goal and obtain the desired planning path.

The above path planning model was applied to generate the ship simulation traffic flow after the completion of area C of the offshore wind farm.

In this study, the generation of the ship model is mainly based on the analysis of historical ship data. Based on a large amount of data in a certain period of time, a cumulative comparison is carried out using the basic idea of the Monte Carlo algorithm for reference.

4.3.1. Ship Attribute Distribution

Based on historical AIS data, we can obtain AIS vessel-type codes and conduct statistical analysis of the ship types. According to the business ownership of the ship and the actual situation of the water area, the ship types are classified and counted. The statistical results of ship type are shown in Figure 15a. The proportion of different ship types is shown in Figure 15b.

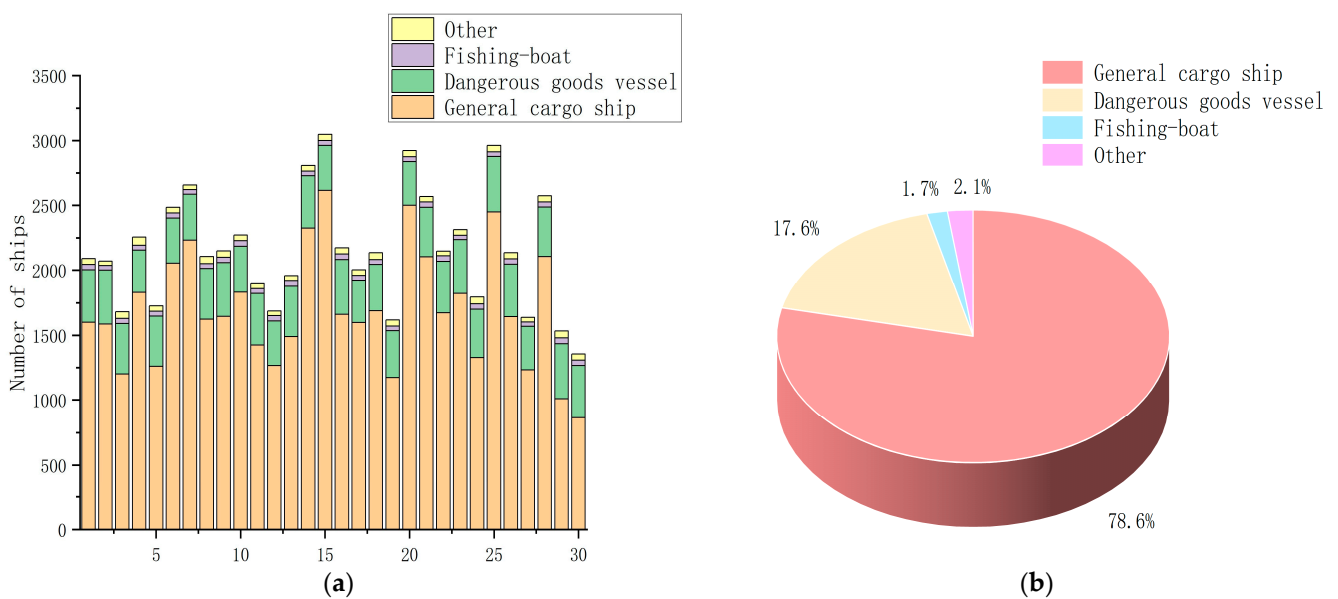


Figure 15. Traffic flow distribution characteristics: (a) ship-type statistics; (b) proportion of different ship types.

According to the statistical results, the share of general cargo ships and dangerous-goods ships in the region is large, at 78.6% and 17.6%, respectively, and the share of fishing boats and other vessels is less than 5%. Therefore, this study is further based on the data rules of general cargo ships and dangerous-goods ships.

Based on the analysis of ship size data in July 2021 in the research area for one month, the probability density histogram of ship length is fitted according to the normal distribution law, and the results are shown in Figure 16.

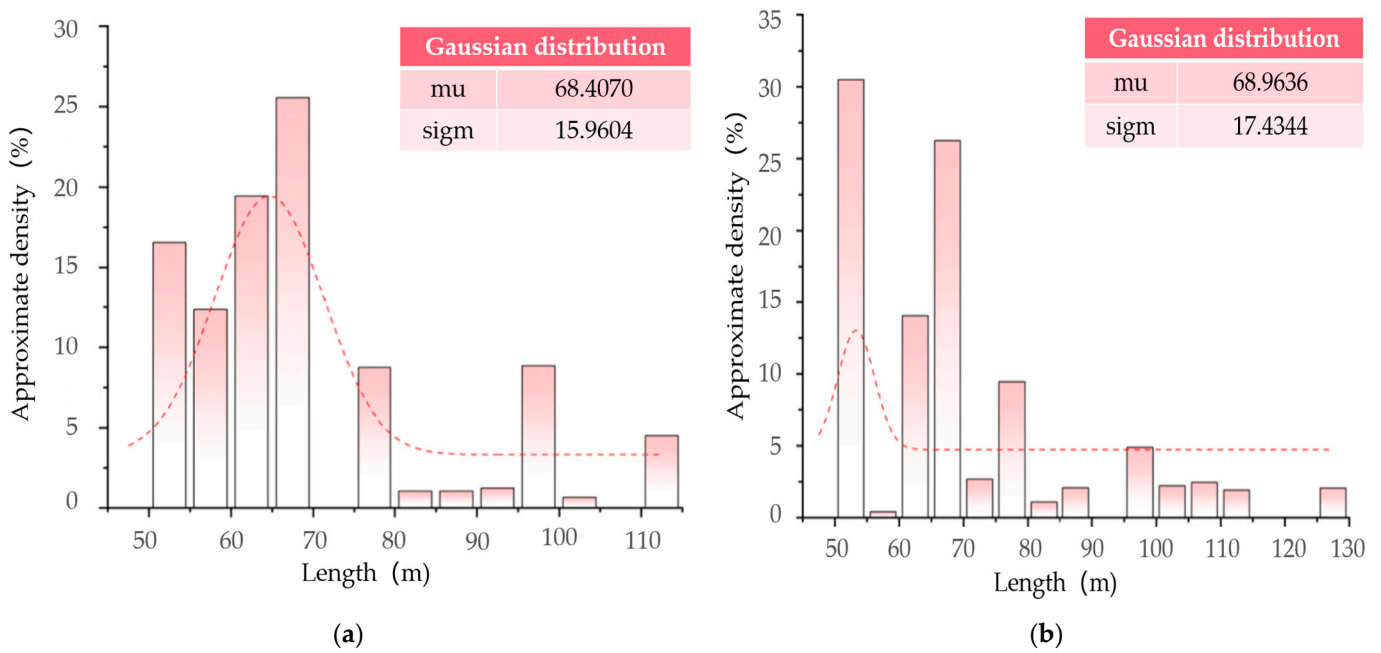


Figure 16. Probability density histogram of ship size: (a) general cargo ship; (b) dangerous-goods ship.

The ship sailing speed data within one month in July 2021 in the study area were analyzed; the probability density histogram of ship sailing speed was fitted according to the normal distribution law, and the results are shown in Figure 17.

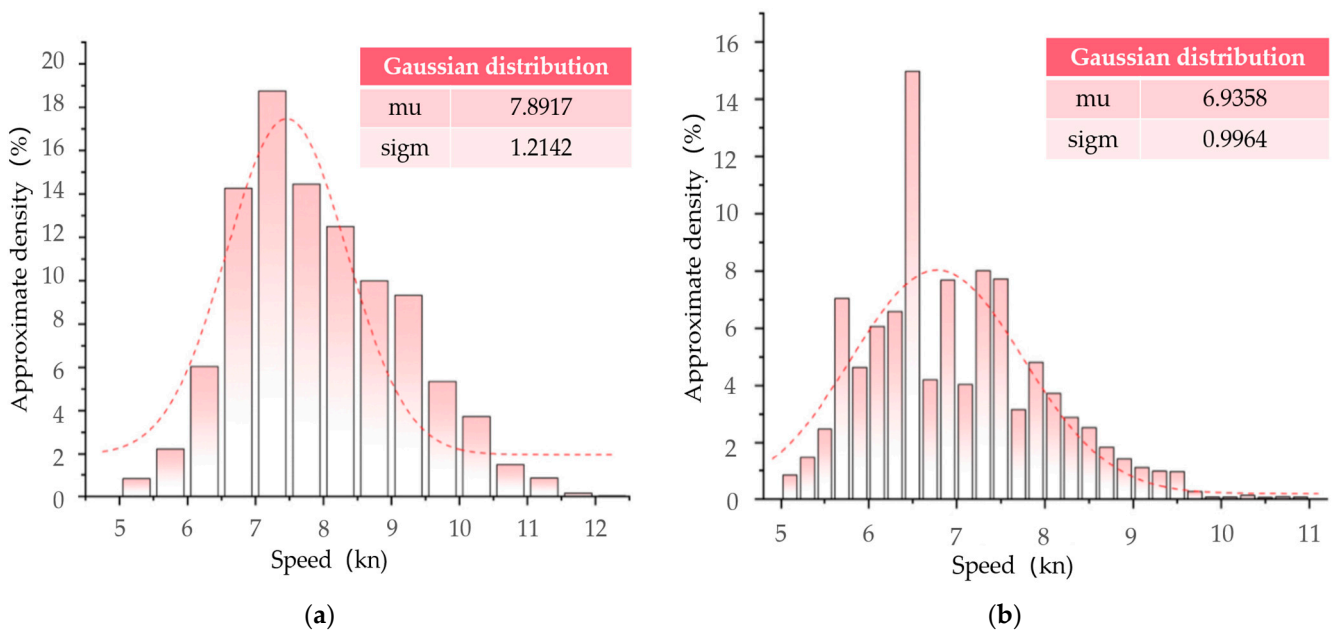


Figure 17. Probability density histogram of ship speed: (a) general cargo ship; (b) dangerous-goods ship.

4.3.2. Simulated Traffic Flow

The simulation time was set to 1 month, and the actual traffic flow generated by historical AIS data was compared. Under the influence of the wind farm, the navigation behavior of ships in the surrounding area changed. Figure 18a shows the actual traffic flow status of the region after changes; Figure 18b shows the traffic flow simulation obtained by using traditional artificial potential field simulations; and Figure 18c shows the traffic flow simulation obtained by using the improved model. It can be seen that the traffic flow

situation in Figure 18b is quite different from the actual traffic flow, while Figure 18c is basically consistent with the actual traffic flow.

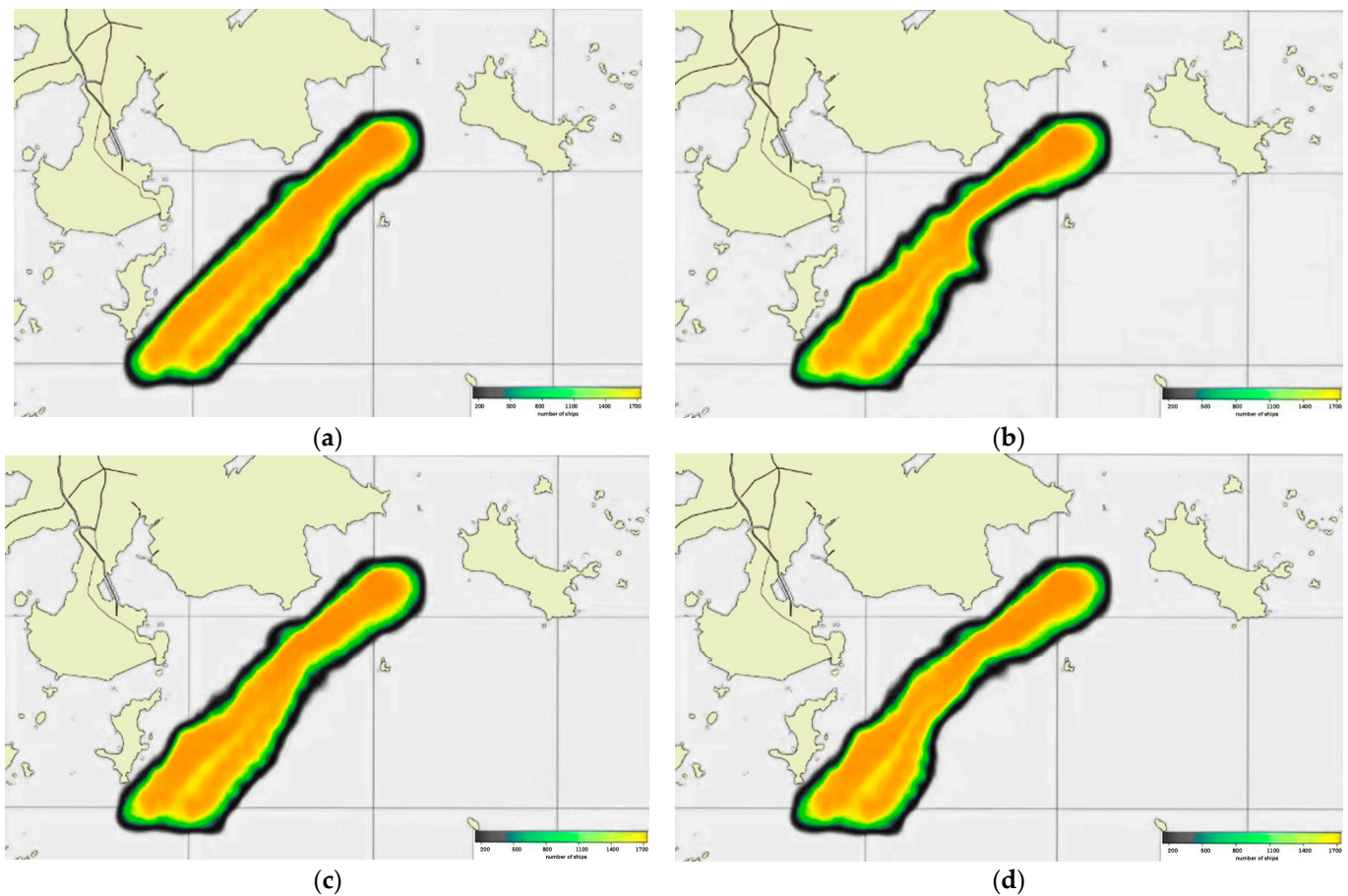


Figure 18. Simulation traffic flow of Pinghaiwan Offshore Wind Farm: (a) actual traffic flow; (b) the traditional artificial potential field method simulates traffic flow; (c) the improved artificial potential field method is used to simulate traffic flow; and (d) simulation traffic flow (when zone E is completed).

Table 3 shows the ratio and relative error of the traffic volume of each route in the total traffic volume in the simulation data and actual data. After comparison, it is found that the relative error is within the permissible range, and the simulation results of ship traffic can reproduce the ship traffic in the water area. The model is feasible for the simulation of ship traffic flow.

Table 3. The proportion of ship traffic volume on each route.

Course	Emulation	Actual
General cargo ship	17.6%	16.1%
Dangerous-goods ship	15.8%	14.2%

Based on the analysis of the existing AIS historical data, the existing traffic flow path was the most cost-effective and safe traffic flow state before the completion of area E, and the figure shows the actual traffic flow before the completion of area E of the offshore wind farm. The planned location of zone E of the offshore wind farm is shown in Table 4.

Table 4. Planned location of area E of offshore wind farm.

Beacon Number	Position
The vertices 1	25°6′49.8″ N, 119°17′02.5″ E
The vertices 2	25°3′09.2″ N, 119°20′35.2″ E
The vertices 3	25°1′18.3″ N, 119°14′16.3″ E
The vertices 4	25°3′02.4″ N, 119°13′03.4″ E

In conclusion, according to the path planning model mentioned above, a thermal map of the simulated ship path after the completion of the E zone of Pinghaiwan Offshore Wind Farm is generated, as shown in Figure 18d. The figure shows the simulated ship traffic flow obtained by the ship traffic simulation model. In general, the simulation model reflects the characteristics of the shipping route in the study area. Under the influence of the E zone of the offshore wind farms, ships will navigate along a route far away from the wind farm, and the customary route will also appear. Moreover, the newly built offshore wind farm has a concentrated distribution in water area E, which has a great impact on ship navigation. The prediction results show that after the wind E area construction characteristics of the ship navigation route and track changed significantly, the ship’s track width was compressed, the routes and ship average density increased, and because of the existence of the collision between the ship and wind farm E area risk pressure, a ship close to the wind farm will usually automatically slow down and must change course to adapt to the new environment of the ship. The simulation results show that after the construction of the wind farm is completed, due to the need to maintain a safe distance, the navigation path of the ship is adjusted accordingly. The construction of offshore facilities will have a certain impact on the navigation behavior of ships in nearby areas, which is in line with our expectation.

5. Discussion

5.1. Feasibility and Contribution

In this study, the artificial potential field model is optimized, and the model is applied to sea traffic flow simulation and prediction. A raster space is constructed by combining the AIS historical data and navigable environmental data in the water area, and a path planning model combining customary routes, offshore wind farms, and moving ships is proposed. In particular, the influence of the historical path on the potential energy field is directly considered in the establishment of the habitual route gravitational field, rather than being restricted by other conditions. With a different inertial path density, the adhesion degree to subsequent path planning is also different. On this basis, the traditional artificial potential field model considering only relative distance is improved, and its mathematical model is optimized.

When multiple force fields are superimposed, or the planned path is close to the obstacle, the traditional artificial potential energy model is prone to the problem of unreachable targets. In this case, the repulsive force and gravity force received by the ship are of the same magnitude and opposite direction, and the total potential energy field is in a stable state, resulting in the ship being unable to approach the target point or escape from local obstacles. To solve this problem, the current artificial potential energy method should be further optimized. Aiming at the above problems, the mathematical model is improved, and the distance factor and constant are introduced into the repulsive force function to restrict the radiation range of the potential field. To confirm the dominance of the global gravitational field, the problem of unreachable targets is avoided, a sufficient potential energy drop is ensured, and the gravitational field coefficient of the customary route is selected and introduced into the equation. The ship path simulation research based on the new manual planning model fully considers the spatiotemporal characteristics of the ship path, provides a certain guarantee for more efficient shipping, and is conducive to the coordination of maritime construction and waterways. At the same time, the new artificial potential field model has feasibility, which can be used in related research and provides a basis for the further study of this path planning model.

5.2. Limitations and Perspectives

The mathematical model of path planning is improved in this study, which solves the problem where the traditional artificial potential field model is trapped in the local optimal solution and cannot reach the destination, and a smoother planned path is obtained. The experimental results show that this method has certain advantages and can provide reference value for follow-up research. The data source in this study is AIS data configured on ships. However, under existing conditions, not all ships can provide real-time data at all times, especially for some small ships or areas where illegal smuggling is rampant and where AIS compliance is poorly enforced. At the same time, AIS data may also have some further issues. However, this is a problem of data sources and data quality. This study does not focus on this aspect. In the future, we can continue to improve and optimize this.

Author Contributions: Conceptualization, Y.S. and X.C.; methodology, Y.S. and X.C.; software, X.C.; validation, Y.S., J.Y. and X.C.; formal analysis, Y.S.; investigation, S.Y.; resources, Y.S.; data curation, X.C.; writing—original draft preparation, X.C.; writing—review and editing, C.C.; visualization, X.C.; supervision, Y.S.; project administration, S.Y. All authors have read and agreed to the published version of the manuscript.

Funding: This research was funded by the National Natural Science Foundation of China (No. 52371369), the Key Projects of National Key R & D Program (No. 2021YFB390150), the Natural Science Project of Fujian Province (No. 2022J01323, 2021J01822, 20230019), the Fuzhou-Xiamen-Quanzhou Independent Innovation Region Cooperated Special Foundation (No. 3502ZCQXT2021007).

Institutional Review Board Statement: Not applicable.

Informed Consent Statement: Not applicable.

Data Availability Statement: The data presented in this study are available on request from the corresponding author.

Conflicts of Interest: The authors declare no conflicts of interest.

References

1. Wenbin, X.; Jingbo, W.; Kaiwen, Z.; Huanhuan, L.; Yan, L.; Zaili, Y. A hierarchical methodology for vessel traffic flow prediction using Bayesian tensor decomposition and similarity grouping. *Ocean Eng.* **2023**, *286*, 115678.
2. Rui, H.; Cuijuan, Z.; Yunpeng, X.; Xingyu, L.; Song, Z.; Yanbing, L. Deep spatio-temporal 3D dilated dense neural network for traffic flow prediction. *Expert Syst. Appl.* **2024**, *237*, 121394.
3. Yu, X.; Bao, Y.-X.; Shi, Q. STHSGCN: Spatial-temporal heterogeneous and synchronous graph convolution network for traffic flow prediction. *Heliyon* **2023**, *9*, e19927. [[CrossRef](#)] [[PubMed](#)]
4. Ye, Y.; Xiao, Y.; Zhou, Y.; Li, S.; Zang, Y.; Zhang, Y. Dynamic multi-graph neural network for traffic flow prediction incorporating traffic accidents. *Expert Syst. Appl.* **2023**, *234*, 121101. [[CrossRef](#)]
5. Yi, X.; Liangzhe, H.; Tongyu, Z.; Leilei, S.; Bowen, D.; Weifeng, L. Generic Dynamic Graph Convolutional Network for traffic flow forecasting. *Inf. Fusion* **2023**, *100*, 101946.
6. Chai, W.; Zheng, Y.; Tian, L.; Qin, J.; Zhou, T. GA-KELM: Genetic-algorithm-improved kernel extreme learning machine for traffic flow forecasting. *Mathematics* **2023**, *11*, 3574. [[CrossRef](#)]
7. Redhu, P.; Kumar, K. Short-term traffic flow prediction based on optimized deep learning neural network: PSO-Bi-LSTM. *Phys. A Stat. Mech. Its Appl.* **2023**, *625*, 129001.
8. Lu, J. An efficient and intelligent traffic flow prediction method based on LSTM and variational modal decomposition. *Meas. Sens.* **2023**, *28*, 100843. [[CrossRef](#)]
9. Yu, W.; Huang, X.; Qiu, Y.; Zhang, S.; Chen, Q. GSTC-Unet: A U-shaped multi-scaled spatiotemporal graph convolutional network with channel self-attention mechanism for traffic flow forecasting. *Expert Syst. Appl.* **2023**, *232*, 120724. [[CrossRef](#)]
10. Xie, Y.; Xiong, Y.; Zhang, J.; Chen, C.; Zhang, Y.; Zhao, J.; Jiao, Y.; Zhao, J.; Zhu, Y. Temporal super-resolution traffic flow forecasting via continuous-time network dynamics. *Knowl. Inf. Syst.* **2023**, *65*, 4687–4712. [[CrossRef](#)]
11. Lazarowska, A. Ship's trajectory planning for collision avoidance at sea based on ant colony optimisation. *J. Navig.* **2015**, *68*, 291–307. [[CrossRef](#)]
12. Szlapczynski, R. Evolutionary planning of safe ship tracks in restricted visibility. *J. Navig.* **2015**, *68*, 39–51. [[CrossRef](#)]
13. Feng, S.; Qian, Y.; Wang, Y. Collision avoidance method of autonomous vehicle based on improved artificial potential field algorithm. *Proc. Inst. Mech. Eng. Part D J. Automob. Eng.* **2021**, *235*, 3416–3430. [[CrossRef](#)]
14. Chang, Z.; Zhang, Z.; Deng, Q.; Li, Z. Route planning of intelligent bridge cranes based on an improved artificial potential field method. *J. Intell. Fuzzy Syst.* **2021**, *41*, 4369–4376. [[CrossRef](#)]

15. Zha, M.; Wang, Z.; Feng, J.; Cao, X. Unmanned vehicle route planning based on improved artificial potential field method. *J. Phys. Conf. Ser.* **2020**, *1453*, 012059. [[CrossRef](#)]
16. Rostami, S.M.H.; Sangaiah, A.K.; Wang, J.; Liu, X. Obstacle avoidance of mobile robots using modified artificial potential field algorithm. *EURASIP J. Wirel. Commun. Netw.* **2019**, *2019*, 1–19. [[CrossRef](#)]
17. Song, J.; Hao, C.; Su, J. Path planning for unmanned surface vehicle based on predictive artificial potential field. *Int. J. Adv. Robot. Syst.* **2020**, *17*, 1729881420918461. [[CrossRef](#)]
18. Jiang, Q.; Cai, K.; Xu, F. Obstacle-avoidance path planning based on the improved artificial potential field for a 5 degrees of freedom bending robot. *Mech. Sci.* **2023**, *14*, 87–97. [[CrossRef](#)]
19. Duan, Y.; Yang, C.; Zhu, J.; Meng, Y.; Liu, X. Active obstacle avoidance method of autonomous vehicle based on improved artificial potential field. *Int. J. Adv. Robot. Syst.* **2022**, *19*, 17298806221115984. [[CrossRef](#)]
20. Cahyadi, A.; Darmawan, E.; Dewanto, W.; Ardiyanto, I. Application of artificial potential field for coverage control with collision avoidance under sensing constraints. *J. Control Autom. Electr. Syst.* **2020**, *31*, 304–318. [[CrossRef](#)]
21. Zhou, H.; Zhou, S.; Yu, J.; Zhang, Z.; Liu, Z. Trajectory optimization of pickup manipulator in obstacle environment based on improved artificial potential field method. *Appl. Sci.* **2020**, *10*, 935. [[CrossRef](#)]
22. Wang, Y.; Chen, X.; Ran, D.; Zhao, Y.; Chen, Y.; Bai, Y. Spacecraft formation reconfiguration with multi-obstacle avoidance under navigation and control uncertainties using adaptive artificial potential function method. *Astrodynamics* **2020**, *4*, 41–56. [[CrossRef](#)]
23. Park, S.-O.; Lee, M.C.; Kim, J. Trajectory planning with collision avoidance for redundant robots using jacobian and artificial potential field-based real-time inverse kinematics. *Int. J. Control Autom. Syst.* **2020**, *18*, 2095–2107. [[CrossRef](#)]
24. Tong, X.; Yu, S.; Liu, G.; Niu, X.; Xia, C.; Chen, J.; Yang, Z.; Sun, Y. A hybrid formation path planning based on A* and multi-target improved artificial potential field algorithm in the 2D random environments. *Adv. Eng. Inform.* **2022**, *54*, 101755. [[CrossRef](#)]

Disclaimer/Publisher’s Note: The statements, opinions and data contained in all publications are solely those of the individual author(s) and contributor(s) and not of MDPI and/or the editor(s). MDPI and/or the editor(s) disclaim responsibility for any injury to people or property resulting from any ideas, methods, instructions or products referred to in the content.